Interaction between heat wave and urban heat island: A case study in a tropical coastal city, Singapore

As Published: 10.1016/j.atmosres.2020.105134

Publisher: Elsevier BV

Persistent URL: https://hdl.handle.net/1721.1/134365

Version: Original manuscript: author's manuscript prior to formal peer review

Interaction between Heat Wave and Urban Heat Island: A Case Study in a Tropical Coastal City, Singapore

Lup Wai Chew[1], Xuan Liu[2], Xian-Xiang Li[3,4,5,*], Leslie K. Norford[6]

[1]*Center for Environmental Sensing and Modeling, Singapore-MIT Alliance for Research and Technology, Singapore*

[2]*Institute of High Performance Computing, Agency for Science, Technology and Research, Singapore*

[3]*School of Atmospheric Sciences, Sun Yat-sen University, China*

[4]*Southern Marine Science and Engineering Guangdong Laboratory (Zhuhai), China*

[5]*Guangdong Province Key Laboratory for Climate Change and Natural Disaster Studies, Sun Yat-sen University, China*

[6]*Department of Architecture, Massachusetts Institute of Technology, USA*

Received: 28 April 2020

Accepted: 12 July 2020

Highlights

- Provide results for a heat wave in the tropics, which is scarce in the literature
- Ground observations show no heat wave-UHI synergy
- WRF simulation agrees well with observation and shows no heat wave-UHI synergy
- Found no significant change in UHI-contributing factors during the heat wave

[*] Corresponding author: Xian-Xiang Li (lixx98@mail.sysu.edu.cn)

Abstract

Heat waves are unusually high temperature events over consecutive days and may cause adverse impacts such as morbidity and mortality. The interaction between heat waves and urban heat island (UHI) effects has remained a subject of debate, as some studies prove heat wave-UHI synergy while others do not. Furthermore, heat waves affect tropical cities more severely than mid-latitude cities, but there is a disproportionate lack of heat wave studies focusing on tropical cities. We attempt to narrow this gap by studying the heat wave in Singapore in April 2016 using ground observations and the Weather Research and Forecasting (WRF) model. Compared to non-heat wave days, the ground observations show that daytime temperatures can be 3 °C higher during the heat wave. Despite the temperature spike, the UHI intensity is not amplified during the heat wave, maintaining its peak near 2.5 °C during both heat wave and non-heat wave periods. WRF simulation results also agree well with measurements and predict UHI peaks near 2.5 °C during both periods, showing no heat wave-UHI synergy. The spatially averaged UHI intensity also shows no such synergy. There is no significant change of wind speed, soil moisture availability or heat storage flux during the heat wave. Therefore, the lack of heat wave-UHI synergy in our study is consistent with current understanding of factors contributing to UHI. This study shows that the heat wave-UHI interaction in a tropical city can be different from that in cities in the temperate climate zone and more studies should be conducted in tropical cities, which are projected to suffer larger impacts of increasing heat stress.

Keywords: heat wave-UHI synergy, ground observations, WRF, tropics, extreme temperature

1. Introduction

Heat waves are extreme heat events lasting for consecutive days. Heat waves bring severe economic, societal, agricultural and health consequences. For example, the deadly heat waves in Chicago in 1995 (Whitman et al., 1997) and Paris in 2003 (Dousset et al., 2011) were estimated to cause 514 and 4,867 heat-related deaths, respectively. The heat wave in April 2016 in Southeast Asia greatly reduced food supplies from Malaysia and the price of vegetables in Singapore spiked (Lin, 2016). Heat waves also strain the infrastructure in dense cities (Li, 2018; Miller et al., 2008). Due to their adverse impacts, numerous studies have been performed to characterize, analyze, and predict heat waves using observations (Perkins et al., 2012), reanalysis data (Li, 2020), regional climate models (Fischer and Schär, 2010), and global circulation models (Meehl and Tebaldi, 2004).

Heat waves are projected to occur more frequently and more intensely, last longer, and cause higher mortality under enhanced greenhouse gas emission conditions (Coumou and Rahmstorf, 2012; Guo et al., 2018; Meehl and Tebaldi, 2004). Heat waves could also exacerbate the urban heat island (UHI) effect (Founda and Santamouris, 2017; Li and Bou-Zeid, 2013) by altering the sensible and latent heat unsymmetrically (D. Li et al., 2015) and changing the wind speeds (D. Li et al., 2016). Nevertheless, the coupling between heat waves and UHI effect has not been fully understood and remains a subject of debate.

On one hand, many researchers have reported synergistic interactions between heat waves and UHI. Zhao et al. (2018) reported that the UHI intensities averaged across 50 cities in the United States were 0.4 to 0.6 °C higher during heat waves. In the Northeastern United States, Ramamurthy and Bou-Zeid (2017) found that the UHI intensities in New York City, Washington D.C. and Baltimore were amplified by 1-2°C during the 2016 heat waves, but no such amplification was found in Philadelphia. Other studies on New York City (Ramamurthy et al., 2017) and Washington, D.C. (Li and Bou-Zeid, 2013) also reported positive synergy between heat waves and UHI intensities. Schatz and Kucharik (2015) showed that the July 2012 heat wave in Madison, Wisconsin, amplified the UHI intensity and in fact, they found that UHI intensity correlates positively with the daily maximum temperature. Unger et al. (2020) showed that UHI can be amplified by up to three times (from about 1 °C to 3°C) during a heat wave in Szeged, Hungary. Founda and Santamouris (2017) claimed to be the first to study the interaction between heat waves and UHI in a coastal city. They reported that the summer 2016 heat wave in Athens amplified the UHI intensity by up to 3.5 °C. In another coastal city,

Shanghai, Ao et al. (2019) also reported amplification of UHI during heat waves between 2013 and 2018, but with a smaller magnitude of 0.8 °C. Jiang et al. (2019) studied heat waves between 2013 and 2018 in Shanghai, Beijing and Guangzhou and found that heat waves intensified the UHI intensity in Shanghai by 1.0 °C, close to the 0.8 °C reported in Ao et al. (2019). A similar magnitude of UHI amplification was observed in Beijing and Guangzhou (1.2 °C and 0.9 °C, respectively). Other studies of Beijing (He et al., 2020; D. Li et al., 2015) also reported significant synergy between heat waves and UHI intensity.

On the other hand, some researchers found no synergistic interactions between heat waves and UHI. In addition to the aforementioned study of Philadelphia that showed no such synergy (Ramamurthy and Bou-Zeid, 2017), Basara et al. (2010) found that in in Oklahoma City, the UHI intensity during summer 2008 heat wave was similar to that during (non-heat wave) summer 2003 (Basara et al., 2008). Scott et al. (2018) averaged 15 heat waves in Baltimore between 2000 and 2015 as a composite event and found no synergy between heat waves and UHI. Extending the study to 54 cities, they concluded that UHI tends to decrease during heat waves.

The brief literature review not only highlights contradicting results on heat wave-UHI interaction, but also reveals the lack of studies of heat waves in the tropics. Although the projected increase of heat stress is the largest over the tropics (Fischer et al., 2012), most studies of heat waves have been focusing predominantly on mid-latitude cities, especially in North America, Europe and Australia (Argüeso et al., 2016; Mora et al., 2017). Furthermore, Im et al. (2017) has emphasized the need to perform separate studies for different regions due to their unique geographies and climates, yet there have been no studies of heat waves in Singapore or neighboring tropical cities. We aim to narrow this gap by analyzing a heat wave in Singapore in April 2016 and its effects on the UHI intensity.

2. Methodology

2.1 Study Area

Singapore is an island nation with about 700 km^2 land area, located between 1°09'N to 1°29'N, and 103°36'E to 104°25'E. Its climate is classified as equatorial rainforest, fully humid (*Af*) under the Köppen-Geiger climate classification (Kottek et al., 2006). The annual rainfall is 2166 mm, with December marking the heaviest monthly rainfall above 300 mm (Meteorological Service Singapore, 2020). The daily temperature variation is small, with daily minima between 23 °C and 25 °C and daily maxima between 31 °C and 33 °C. The monthly

temperature variation is within a narrow range: the warmest months (May and June) have daily mean temperatures of 27.8 °C, while the coldest months (December and January) have daily mean temperatures of 26.0 °C. The daily relative humidity ranges between 60% in the afternoons and 90% in the early mornings (Meteorological Service Singapore, 2020).

There are 15 weather stations across Singapore providing real-time data on the website of the Meteorological Service Singapore but not all stations are suitable for UHI estimation. As highlighted by Stewart (2011), UHI should be estimated by fewer representative sites instead of more unrepresentative sties. As a "City in a Garden" (Ng, 2019), Singapore has a high green view index (X. Li et al., 2015) of 29.3 %, surpassing some exemplars of green cities such as Vancouver (25.9%) and Amsterdam (20.6%) (Ratti et al., 2016). Although urban greenery is generally beneficial, they render most of the weather stations unsuitable for UHI estimation. To estimate UHI, an urban station should be in a central urban area with 70% or higher impervious surface and 20% or lower vegetation cover within 1 km^2 of the station, while a rural station should be outside urban areas with 65% or higher vegetation cover (Jiang et al., 2019). Among the 15 weather stations, only the Tai Seng station (1°20'24"N, 103°53'16"E) and the Pulau Ubin station (1°25'00"N, 103°58'02"E) satisfy the requirements for an urban and a rural station, respectively, and are thus selected for UHI quantification. Figure 1(a) shows the location of both weather stations and the land use/land cover map in Singapore (Li et al., 2013). Figure 1(b) and Figure 1(c) show the aerial photograph of the surroundings of the Tai Seng station and Pulau Ubin stations, correspond to the compact midrise and dense tree local climate zones, respectively (Stewart and Oke, 2012). The Tai Seng station and the Pulau Ubin station are located at 36 m and 27 m above mean sea level, respectively (both are about 15 m above ground). The weather station data are available at a temporal resolution of five minutes but are averaged every minute. For example, the temperature at 08:05 local time (LT) is averaged between 08:04 and 08:05 LT. The next available temperature is at 08:10 LT, which is averaged between 08:09 and 08:10. Occasionally, the weather stations do not provide any data due to maintenance or equipment failure. The accuracies for temperature, relative humidity (RH) and

wind speed measurements are ±0.2 °C, ±2% RH and ±0.3 m/s, respectively (Meteorological Service Singapore, 2017).

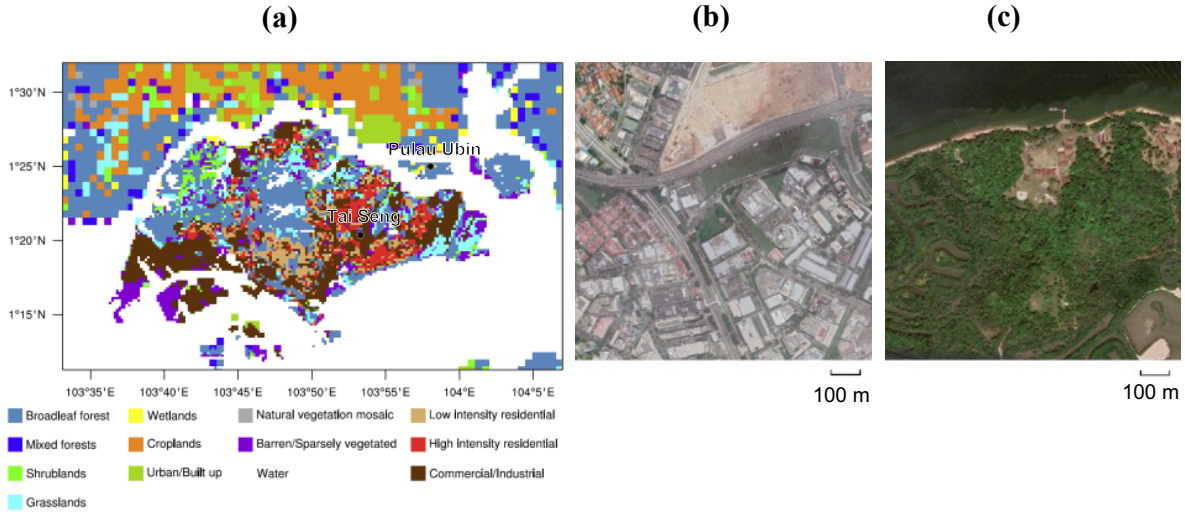

Figure 1. (a) The land use/land cover map of Singapore and the surrounding (from Li et al., 2013) with the two black dots indicating the locations of the urban (Tai Seng) and rural (Pulau Ubin) weather stations. The surroundings of (b) the Tai Seng station and (c) the Pulau Ubin station (both images from Google Map).

2.2 Heat waves in Singapore

The Meteorological Service Singapore defines a heat wave as three or more consecutive days with daily maximum temperatures exceeding 35 °C and daily mean temperatures exceeding 29 °C based on three designated stations with long-term temperature records (Meteorological Service Singapore, 2020). Note that this definition does not include the effects of humidity. The apparent temperature, or the sultriness index (Steadman, 1979), considers both temperature and humidity and is a more representative measure of heat stress on humans, especially in tropical cities. During the 2016 heat wave in Singapore, the Tai Seng station recorded a maximum temperature of 35.3 °C and a relative humidity of 53%, corresponding to an apparent temperature of 43 °C.

There were six heat waves in Singapore since record-keeping began in 1979; three occurred in 1983, one each in 1998, 2010, and 2016 (Timbal et al., 2018). This study focuses on the most recent heat wave on April 17-19, 2016, as data is only available after April 2011 when the Tai Seng station started operating. By comparing the maximum temperatures recorded at the Changi station (the longest operating station since 1982), the heat waves in 1983 recorded a maximum temperature of 35.8 °C, while the heat waves in 1998 and 2010 recorded a maximum temperature of 34.7 °C and 35.5 °C, respectively. These relatively similar

maximum temperatures show that the April 2016 heat wave in our study is representative of all historical heat waves in Singapore.

To compare the UHI magnitude during the heat wave to that of non-heat wave days, a period of "pre-heat wave" and "post-heat wave" are identified before and after the heat wave (Li and Bou-Zeid, 2013). The pre- and post-heat wave periods are April 3-5 and April 24-27, corresponding to three consecutive days with daily mean temperatures lower than 29.8 °C (monthly mean temperature on April 2016 at the Tai Seng station) before and after the heat wave, respectively. Table 1 summarizes the daily maximum and daily mean temperatures at the Tai Seng station during the pre-, heat wave, and post-heat wave periods.

Table 1. Daily maximum and daily mean temperatures at the Tai Seng station during the pre-, heat wave, and post-heat wave periods.

Period	Date	Max temperature (°C)	Mean temperature (°C)
Pre-heat wave	April 3	32.2	29.1
	April 4	32.2	29.4
	April 5	31.5	29.5
Heat wave	April 17	33.9	30.5
	April 18	35.3	31.0
	April 19	33.9	31.0
Post-heat wave	April 24	32.0	29.7
	April 25	33.3	29.6
	April 26	31.9	29.7

2.3 WRF Model Description and Validation

The Weather Research and Forecasting (WRF) model is one of the state-of-the-art regional climate models (Tapiador et al., 2020) and has been successfully applied to simulate many heat wave events (Founda and Santamouris, 2017; Jandaghian and Berardi, 2020a; Li and Bou-Zeid, 2013; Rastogi et al., 2020; Valmassoi et al., 2020). We use WRF version 3.8.1 with the Advanced Research WRF dynamics core developed by the National Center for Atmospheric Research (Skamarock et al., 2008). The Noah land surface model (LSM) provides surface heat fluxes and skin temperatures as the lower boundary conditions. The Noah LSM is coupled to a single-layer urban canopy model (SLUCM) (Kusaka et al., 2001; Kusaka and Kimura, 2004) to model the urban effects on the overlying atmosphere. The urban parameterizations have been studied in detail and validated in Li et al. (2013) and are not repeated here. The land use/land cover type is shown in Figure 1. The urban areas are categorized into three sub-categories, namely low-intensity residential, high-intensity

residential, and commercial/industrial areas. The diurnal profiles of anthropogenic heat data in Quah and Roth (2012) are used. The low-intensity residential, high-intensity residential, and commercial/industrial areas have peak anthropogenic heat of 13, 18, and 113 W m^{-2}, respectively.

The WRF model has five one-way nested domains as shown in Figure 2. The smallest domain (d05) has a grid size of 0.3 km by 0.3 km and a time step of 1 s. The grid ratio is 3 and the time step fractional number is 3, i.e., domain d04 has a grid size of 0.9 km by 0.9 km and a time step of 3 s. The largest domain (d01) has a grid size of 24.3 km by 24.3 km and a time step of 81 s. Note that the fine grid resolution in d05 is in the "terra incognita", or grey zone, in planetary boundary layer (PBL) modelling (Wyngaard, 2004). This means that the momentum and heat fluxes in the PBL are partly resolved, in contrast to traditional PBL parameterizations that cannot resolve any turbulence (Shin and Dudhia, 2016). Previous validation studies on Singapore using a similar fine grid have confirmed that the simulation results agree well with measurements (Li et al., 2013; X.-X. Li et al., 2016; Li and Norford, 2016).

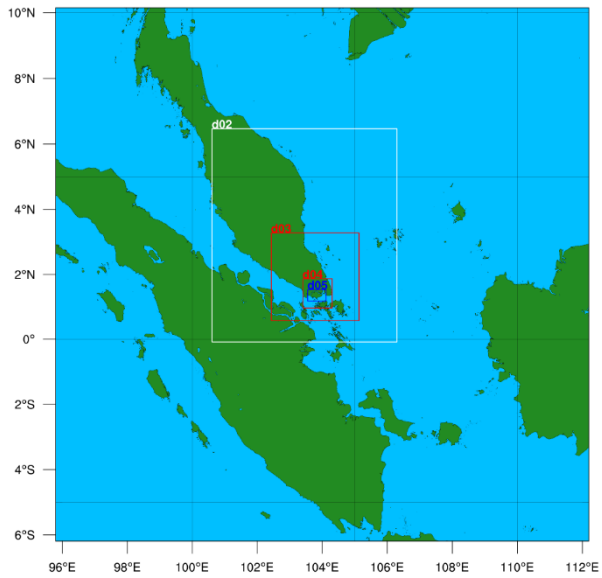

Figure 2. The five nested domains in the WRF model. The smallest domain (d05) is shown in Figure 1 with the land use land cover map.

The Mellor-Yamada-Janjić PBL scheme and the Goddard microphysics scheme are employed. Other physical parameterizations employed are the Rapid Radiative Transfer Model long-wave radiation scheme, the Dudhia short-wave radiation scheme, the Monin-Obukhov surface layer scheme, and the Kain-Fritsch cumulus scheme (only for d01 and d02). The initial

and boundary conditions are obtained from NCEP's Global Data Assimilation System (GDAS) 6-hourly data with 0.25° spatial resolution (National Centers for Environmental Prediction, 2015). The WRF simulations are conducted for the period from 31st March 2016 08:00 LT to 1st May 2016 08:00 LT. The first 16 hours are considered as a ramp-up period and excluded from the data analysis. The simulation results are exported every simulated hour (i.e., every 3600 time steps for d05).

Figure 3 compares the simulated 2-m air temperature, 2-m relative humidity, and 10-m wind speed with measurements at both the rural and urban stations for April 2016. For temperature and relative humidity, Figure 3(a)-(d) show that the simulation captures the diurnal profiles well. The rural station has root mean square errors (RMSEs) of 1.8 °C and 8.7 %, respectively, while the urban station has RMSEs of 1.6 °C and 8.8 %, respectively. Given the various parameterizations adopted, WRF simulations are considered accurate with RMSEs smaller than 2 °C for temperature and 10 % for relative humidity (Ramamurthy et al., 2017). For wind speed, Figure 3(e)-(f) show that WRF consistently overpredicts the wind speeds at both stations, with RMSEs of 1.9 m s^{-1} and 1.6 m s^{-1}, respectively. Simulated wind speed could be different from measurements due to simplification in parameterizing the land surface (Ramamurthy and Bou-Zeid, 2017; Salamanca et al., 2011). However, this does not influence our finding that wind speed is not affected by the heat wave, which will be discussed in Section 3.3.

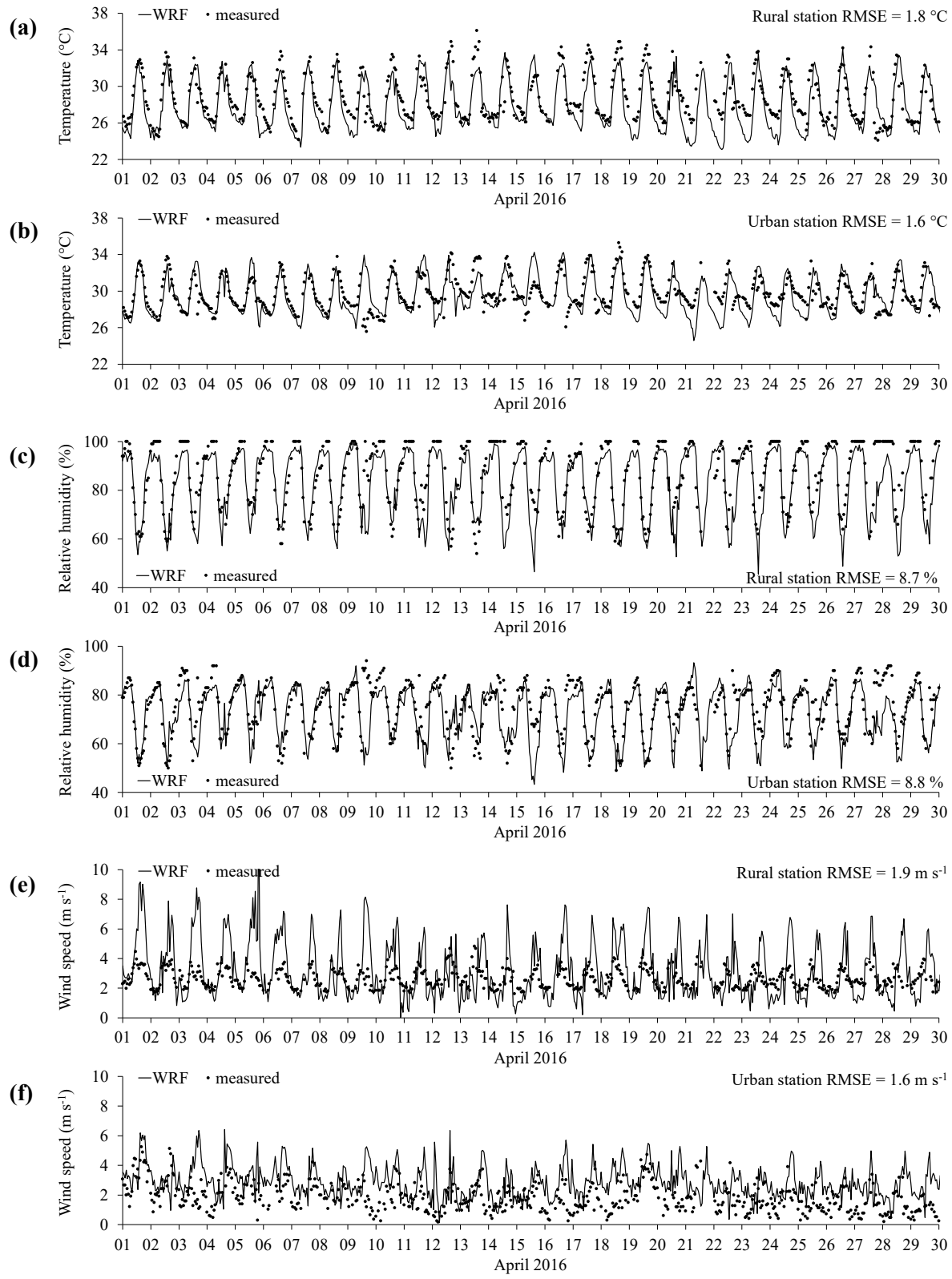

Figure 3. Comparison WRF simulation with measurements and the RMSE at both the rural and urban stations for: (a)-(b) 2-m air temperature, (c)-(d) 2-m relative humidity, and (e)-(f) 10-m wind speed.

2.4 Two Methods to Calculate UHI Intensity

There are two methods to calculate UHI intensity. The first method calculates the UHI intensity as the temperature difference between a selected urban area and a reference rural area. This method is straightforward and calculates the UHI intensity of a specific site. The second method, namely the "urban increment" method, extracts the impact of urbanization by taking the difference between a control case and an experimental case with all urban areas replaced by rural areas (Bohnenstengel et al., 2011). This method has the advantage of showing the spatial distribution of UHI (which will be discussed in Section 3.4.3). To obtain the urban increment of temperature in our study, another WRF simulation is run with all the urban categories replaced by rural category (broadleaf forest as it is the main rural type in Singapore). The original case with urban areas is named "Control Case," while the case with only rural areas is named "Forest Case." The urban increment is then calculated by taking the difference of these two cases (Control Case minus Forest Case). Previous study has verified that both methods provide similar UHI in both the diurnal variation and magnitude (Li et al., 2013).

3. Results and Discussion

The result analysis focuses on three periods: pre-heat wave (April 3-5), heat wave (April 17-19) and post-heat wave (April 24-26). For each of these periods, all parameters (2-m air temperature, 2-m relative humidity and 10-m wind speed) are averaged over the three selected days. For example, the pre-heat wave 2-m air temperature is the average temperature of April 3, 4, and 5.

3.1 2-m air temperature

Figure 4 shows the 3-day averaged 2-m air temperature for both the rural and urban stations during the pre-heat wave, heat wave, and post-heat wave periods. The measurements (labelled "mea") are shown as open symbols while the WRF simulations are shown as lines. For the rural station, the measurements show no significant difference among the three periods except between 1200 and 1900 LT, where temperatures during the heat wave could be 3 °C higher than those during pre-heat wave and post-heat wave. The WRF simulation captures the diurnal profile well, but underpredicts both daytime and nighttime temperatures during the heat wave and nighttime temperatures during the post-heat wave. For the urban station, the measurements show no significant difference among the three periods except between 1100 and 1800 LT, where temperatures during the heat wave could be 3 °C higher than those during pre-heat wave and post-heat wave. The WRF simulation captures the diurnal profile of the

urban station well, but shows a similar bias as observed at the rural station, where the temperatures tend to be underpredicted during the heat wave and post-heat wave, especially between 0000 and 1100 LT.

Overall, Figure 4 suggests that the heat wave only increases the temperatures between 1200 and 1900 LT at both stations. During the heat wave, both the rural and urban stations recorded the coolest hour at 0700 LT, while the warmest hour was recorded at 1500 LT. WRF results show good agreement with measurements with some biases, but the biases have the same sign so they partially cancel each other in the urban heat island intensity calculation, which will be further discussed in Section 3.4.

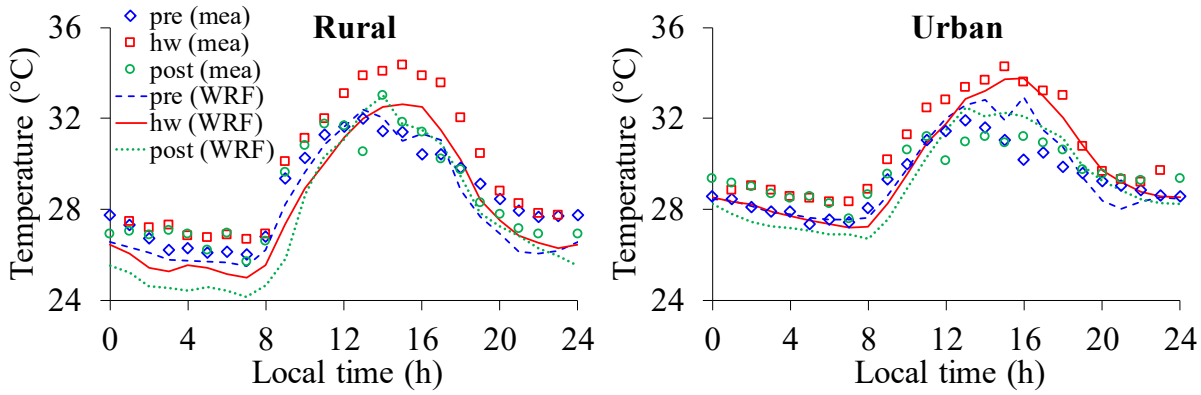

Figure 4. Hourly temperature (3-day averaged) during the pre-heat wave ("pre"), heat wave ("hw"), and post-heat wave ("post") periods for both rural and urban stations. Open symbols ("mea") are from measurements and lines ("WRF") are from WRF simulation.

3.2 2-m Relative Humidity

Figure 5 shows the 3-day averaged 2-m relative humidity for both the rural and urban stations during the pre-heat wave, heat wave, and post-heat wave periods. Measured relative humidity shows a distinctive diurnal profile, with the rural stations recorded about 60-70% relative humidity during daytime and up to 100% relative humidity during nighttime. The urban station has a similar profile, but the peak is lower at 90%. The only significant difference among the three periods is observed between 1200 and 1900 LT, where the relative humidity is lower during the heat wave compared to that during pre-heat wave and post-heat wave. WRF simulation captures the same profiles and peaks at both stations, confirming WRF's capability to accurately simulate relative humidity.

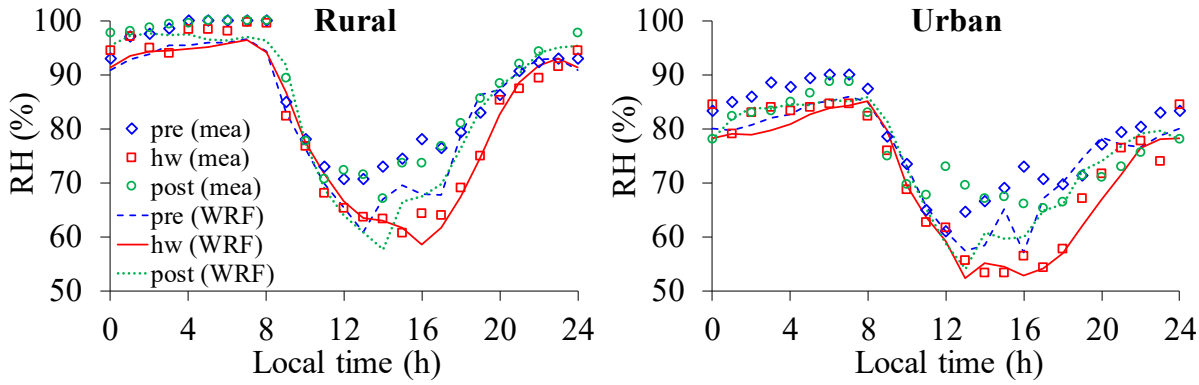

Figure 5. Hourly relative humidity (3-day averaged) during the pre-heat wave ("pre"), heat wave ("hw"), and post-heat wave ("post") periods for both rural and urban stations. Open symbols ("mea") are from measurements and lines ("WRF") are from WRF simulations.

3.3 10-m Wind Speed

Figure 6 shows the 3-day averaged 10-m wind speed for both the rural and urban stations during the pre-heat wave, heat wave, and post-heat wave periods. From the measurements in Figure 6, there is no reduction of wind speed at both stations during the heat wave in this study. Despite the over-prediction of wind speed especially at the rural station, the WRF simulation shows a similar profile during the pre-heat wave, heat wave and post-heat wave periods. In other words, both measurements and simulation suggest that wind speeds are not influenced during the heat wave.

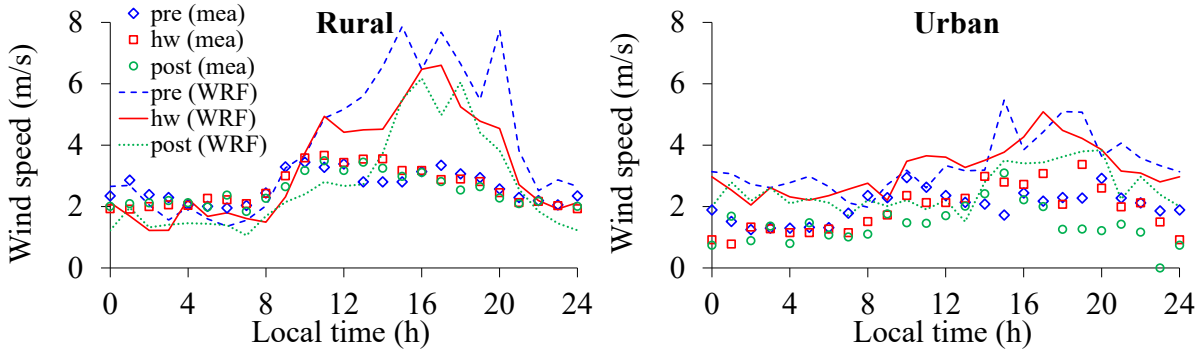

Figure 6. Hourly wind speeds (3-day averaged) during the pre-heat wave ("pre"), heat wave ("hw"), and post-heat wave ("post") periods for both rural and urban stations. Open symbols ("mea") are from measurements and lines ("WRF") are from WRF simulations.

3.4 UHI Intensity

3.4.1 UHI Intensity Based on Two Stations

The UHI intensities are calculated by taking the temperature difference between the urban and rural stations in Figure 4 (the first method discussed in Section 0). Figure 7 compares

the 3-day averaged UHI intensities during the pre-heat wave, heat wave, and post-heat wave periods. Overall, the measurements show no apparent synergy between UHI intensity and the heat wave. The peaks during pre-heat wave, heat wave, and post-heat wave periods are equally high, reaching about 2.5 °C. The diurnal profiles are also similar, with the peak UHI intensities recorded at midnight and zero or negative UHI intensities recorded during the daytime. The WRF simulation correctly predicts the diurnal profile and the peak UHI at about 2.5 °C. More importantly, there is no significant deviation among the three UHI profiles from WRF simulation, consistent with the measurements that show no synergy between UHI intensity and the heat wave.

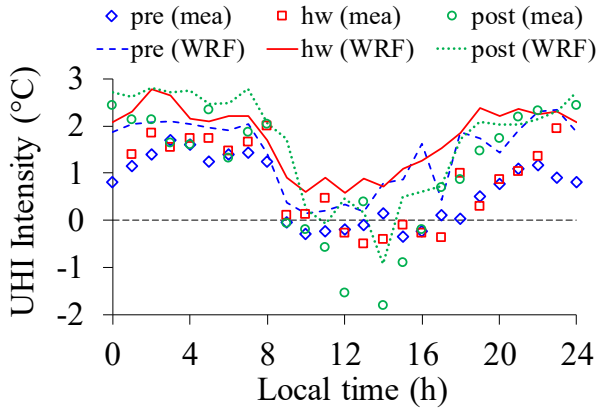

Figure 7. UHI intensity at the urban station during the pre-heat wave ("pre"), heat wave ("hw"), and post-heat wave ("post") period. Open symbols ("mea") are from measurements and lines ("WRF") are from WRF simulations.

3.4.2 Spatially Averaged UHI Intensity

The UHI profiles in Figure 7 is calculated based on only two points (the rural and urban stations). With the WRF model shown to be accurately predicting the 2-m air temperatures, we can use the validated WRF simulation to plot the temperature distribution over all of Singapore. The spatially averaged UHI profiles can then be extracted from these temperature maps. Figure 8 shows the temperature maps during the pre-heat wave, heat wave, and post-heat wave periods. For brevity, only the temperature maps at 0700 LT and 1500 LT are plotted, as they correspond to the coolest and warmest hour during the heat wave.

Figure 8(a) shows that at 0700 LT, the southern part of Singapore is consistently warmer than the northern part for all three periods. Referring to the land use/land cover map in Figure 1, the warmer regions correspond to urban areas, while the cooler regions correspond to rural areas. There is no significant difference of temperature distribution among the pre-heat

wave, heat wave, and post-heat wave periods. In contrast, at 1500 LT, Figure 8(b) shows a distinctive temperature distribution during the heat wave compared to those during the pre-heat wave and post-heat wave periods. During the pre-heat wave period, most areas have temperatures lower than 33 °C, whereas during the heat wave, almost the entire Singapore (except the southernmost part) has high temperatures above 33 °C. During the post-heat wave period, only the norther part of Singapore experiences high temperatures (but not as high as the temperatures during the heat wave).

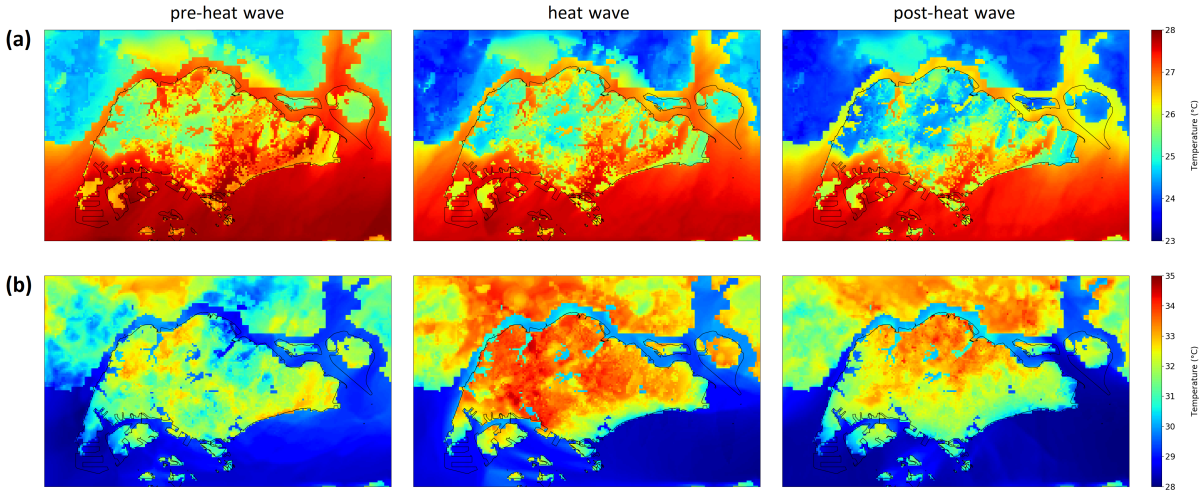

Figure 8. Three-day averaged 2-m air temperature during pre-heat wave, heat wave, and post-heat wave at (a) 07:00 LT and (b) 15:00 LT. Note the different scales for (a) and (b).

With temperature maps such as those in Figure 8, we can derive the spatially averaged UHI profiles. There are three urban categories in the WRF model: low-intensity residential, high-intensity residential, and commercial or industrial (see Figure 1 for the land use/land cover map). Broadleaf forest is taken as the rural category because it is the main rural type in Singapore. The average temperature of each category is calculated by spatially averaging the temperatures of all grids corresponding to the category. For example, the average temperature of the rural category is calculated by spatially averaging the temperatures of all broadleaf forest grids. The spatially averaged UHI is then calculated as the difference of (spatially averaged) temperatures between each urban category and the rural category.

Figure 9(a)-(c) show the spatially averaged UHI intensities of low-intensity residential areas, high-intensity residential areas, and commercial or industrial areas, respectively. No apparent synergy between UHI intensity and heat wave is observed. All three urban categories observed a similar diurnal profile: UHI intensities fluctuate near zero between 1000 and 1600 LT, rise between 1600 and 1900 LT, stay near their peaks between 1900 and 0700 LT, and

decrease between 0700 and 1000 LT. Low-intensity residential areas have the lowest UHI peak at about 1 °C, while the commercial or industrial areas have the highest UHI peaks at about 2 °C. This is expected because the commercial or industrial areas have anthropogenic heat about an order of magnitude higher than that of the residential areas. The urban station used to calculate the measured UHI intensity is located in an industrial area. The UHI profiles in Figure 9(c) resemble the measured UHI profiles in Figure 7, justifying that the two selected stations are representative of rural and urban (commercial or industrial) sites.

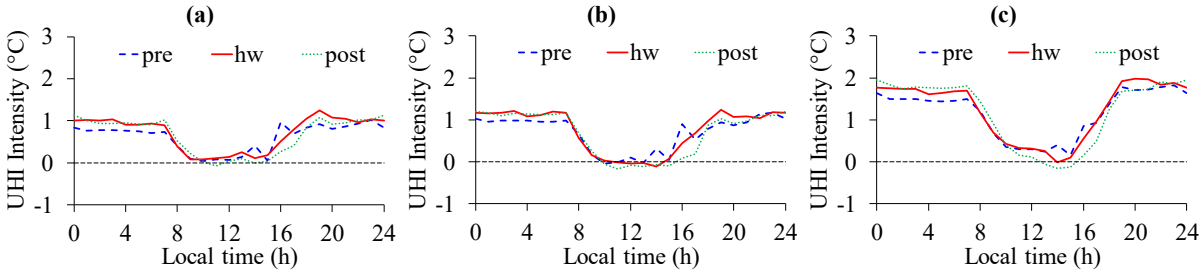

Figure 9. Spatially averaged profiles of UHI intensity obtained from WRF during the pre-heat wave ("pre"), heat wave ("hw"), and post-heat wave ("post") period for: (a) low-intensity residential, (b) high-intensity residential, and (c) commercial/industrial.

3.4.3 UHI Intensity Calculated by the Urban Increment Method

The temperature maps in Figure 8 do not directly show the spatial distribution of UHI. Although we can refer to Figure 1 to identify urban and rural areas and then refer back to Figure 8 for the corresponding temperatures at these areas, this process is tedious. To visualize the spatial distribution of UHI, we use the urban increment method (outlined in Section 0) to calculate the UHI intensity for the entire Singapore Island. Figure 10 plots the spatially averaged urban increment of temperature. Compared to the UHI intensity in Figure 9, the urban increment of temperature in Figure 10 shows a similar diurnal profile. Although the latter has slightly higher nighttime peaks, the conclusion that no synergy between UHI intensity and heat wave still holds, since there is no apparent difference among the pre-heat wave, heat wave, and post-heat wave periods. The close resemblance of Figure 9 and Figure 10 verifies that the urban increment of temperature can be used as an indicator of UHI intensity. We can then plot the maps of urban increment to visualize the spatial distribution of UHI intensity.

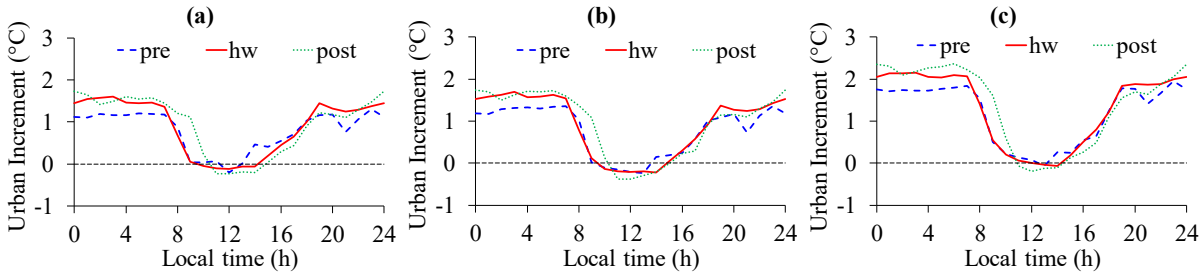

Figure 10. The "urban increment" (i.e., Control Case minus Forest Case) of spatially averaged temperatures during the pre-heat wave ("pre"), heat wave ("hw"), and post-heat wave ("post") period for: (a) low-intensity residential, (b) high-intensity residential, and (c) commercial/industrial areas.

Figure 11 compares the 3-day averaged UHI intensity calculated by the urban increment method during pre-heat wave, heat wave, and post-heat wave periods. For brevity, only the UHI maps at 0700 LT and 1500 LT results are shown. At 0700 LT, Figure 11(a) shows that overall, all three maps show about the same UHI distribution and magnitude. Urban areas, especially those at the southern part of Singapore, consistently display positive UHI intensity up to 3 °C. There is no amplification of UHI intensity during the heat wave. At 1500 LT, Figure 11(b) shows that although there are some areas with observable UHI effects (could be either positive or negative), these areas are small and overall, no significant difference is observed among the three periods. In summary, Figure 11 confirms that there is no synergy between UHI intensity and heat wave for the April 2016 heat wave in Singapore.

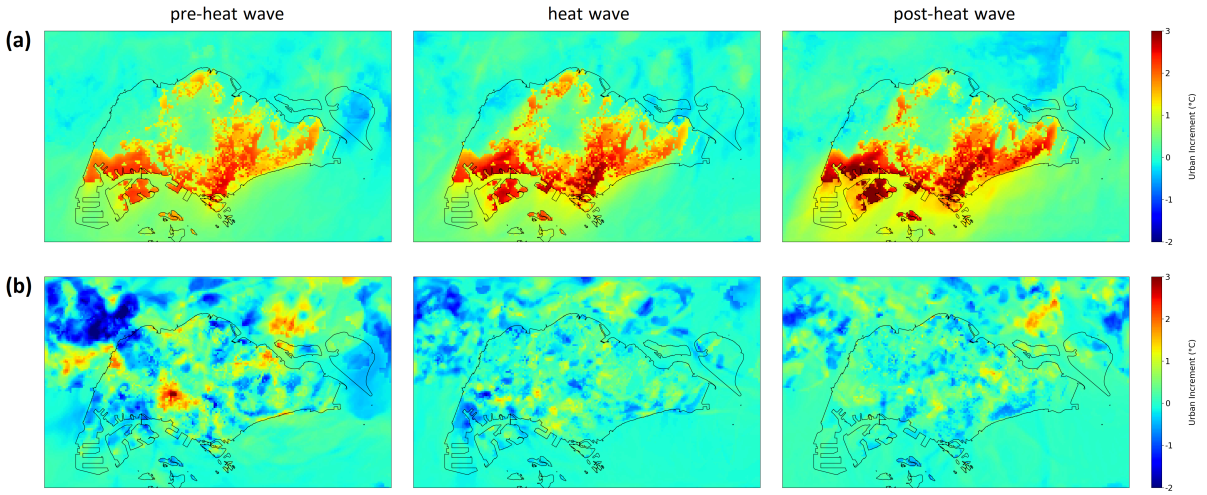

Figure 11. Three-day averaged urban increment of 2-m air temperature (Control Case – Forest Case) during pre-heat wave, heat wave, and post-heat wave periods at (a) 07:00 LT and (b) 15:00 LT.

3.5 Contributing Factors of UHI

The UHI phenomenon is complex and involves many coupled factors, including synoptic conditions, urban population, vegetation fraction, building materials, sky view factor,

and many more (Rizwan et al., 2008; Stewart, 2019). Since our study spans only one month (April 2016), many of these factors such as population and building materials do not change over the entire study period and can be excluded from the analysis of heat wave-UHI synergy. We explore four major factors that could affect the UHI intensity: wind speed, soil moisture availability, heat storage flux, and the roughness lengths and surface resistance (Li and Bou-Zeid, 2013, 2014; Ramamurthy et al., 2017) to investigate why there is no observable synergy between the April 2016 heat wave in Singapore and the UHI effect.

3.5.1 Wind Speed

As shown in Figure 6, wind speeds during the pre-heat wave, heat wave and post-heat wave have the same diurnal profile. Wind speed during daytime is slightly higher than that during nighttime. There is no significant deviation of wind speed during the heat wave compared to the pre- and post-heat wave periods. Contrary to other studies showing reduction in wind speed during heat waves and the associated heat wave-UHI amplification (Ao et al., 2019; Li and Bou-Zeid, 2013; Ramamurthy et al., 2017), no reduction of wind speed is observed during the heat wave in our study. As reduced wind speed can enhance the UHI intensity (Li and Bou-Zeid, 2013), the lack of heat wave-UHI synergy in our study is consistent with no observable reduction in wind speed.

3.5.2 Soil Moisture Availability

Low soil moisture availability can lead to more frequent, longer-lasting heat waves (Hirschi et al., 2011) and amplifies the temperature anomalies during heat waves (Fischer et al., 2007). Figure 12 plots the spatially averaged top (0-10 cm) volumetric soil moisture (unit m^3m^{-3}) calculated in WRF for all three urban categories and the rural category. During the pre-heat wave period, all four categories have about the same soil moisture (about 0.25 m^3m^{-3}). Starting from April 13, the urban areas lose moisture faster than the rural areas as indicated by the steeper negative slope. During the heat wave, the urban categories have a soil moisture of about 0.23 m^3m^{-3}, while the soil moisture of rural areas is about 0.25 m^3m^{-3}, i.e., the urban-rural difference soil moisture deficit is 0.02 m^3m^{-3}. During the post-heat wave period, the soil moisture of the urban areas drops to 0.20 m^3m^{-3}, while the soil moisture of the rural areas drops to 0.23 m^3m^{-3}, i.e., the urban-rural soil moisture deficit is 0.03 m^3m^{-3}. The urban-rural soil moisture deficit during the heat wave (0.02 m^3m^{-3}) is not significantly different than those during the pre-heat wave period (< 0.01 m^3m^{-3}) and the post-heat wave period (0.03 m^3m^{-3}) and therefore, the UHI intensity is not amplified during the heat wave. As a comparison to the

2006 heat wave in New York City, the urban-rural soil moisture deficit during the heat wave can exceed 1.0 m^3m^{-3}, thus triggering an amplification of UHI intensity (Ramamurthy et al., 2017).

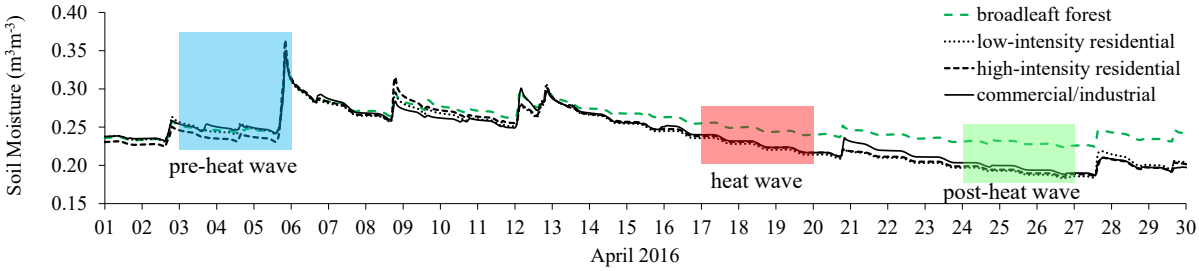

Figure 12. Spatially averaged top soil moisture of the rural (broadleaf forest) and urban categories (low-intensity residential, high-intensity residential, and commercial/industrial) in April 2016.

3.5.3 Heat Storage Flux

The difference in heat storage flux across urban and rural areas influences the UHI intensity. In urban areas, buildings and other urban structures store the heat during daytime and release the heat at nighttime. As urban areas are mostly covered with impervious surfaces, most of the stored heat is released as sensible heat and induces the UHI effect. For example, in New York City, heat storage flux can induce a UHI intensity up to 6 °C (Ramamurthy et al., 2017). Therefore, the UHI intensity is expected to increase if the heat storage flux across the urban areas is amplified during a heat wave.

The heat storage flux is a component in the surface energy balance, where $Q^* + Q_F = Q_H + Q_E + \Delta Q_S$. Here, Q^* is the net all-wave radiation, Q_F is the anthropogenic heat, Q_H is the sensible heat flux, Q_E is the latent heat flux, and ΔQ_S is the net heat storage flux (Oke, 1988). Figure 13 plots the spatially averaged ΔQ_S, Q^*, Q_H, and Q_E for the rural (broadleaf forest) and urban categories (low-intensity residential, high-intensity residential, and commercial/industrial areas). ΔQ_S is expected to increase during heat waves. For example, Sun et al. (2017) summarized four studies of heat waves in different cities: Beijing (Wang et al., 2014), Lodz (Offerle et al., 2006), London (Kotthaus and Grimmond, 2014), and Swindon (Ward et al., 2013). They concluded that all four cities (none is in the tropics) have increased ΔQ_S during heat waves. Interestingly, our study in Singapore shows otherwise: ΔQ_S across both urban and rural areas remains relatively constant. During daytime, the ΔQ_S peaks remain unchanged during the heat wave compared to those during the pre- and post-heat wave periods. During nighttime when the stored heat is released (a main contributor to UHI), the magnitude

of ΔQ_S also shows no significant difference between the heat wave and non-heat wave periods, consistent with no amplification in both observed and simulated UHI intensity.

To understand the relatively unchanged ΔQ_S during heat wave, we look at other components in the surface energy balance. During the heat wave, Q^* is up to 100 Wm^{-2} higher for the rural category and up to 170 Wm^{-2} higher for the urban categories. This higher Q^* is likely due to an increase in the incoming shortwave radiation with clear sky conditions during heat waves (Black et al., 2004). This higher Q^* increases the overall surface energy budget for both urban and rural categories. The higher Q^* is distributed to Q_H in urban areas and to Q_E in rural areas, as shown by the Q_H and Q_E plots in Figure 13. All three urban categories show an increase in Q_H during the heat wave, while the rural category shows an increase in Q_E. Overall, the additional Q^* is partitioned to Q_H and Q_E without altering ΔQ_S.

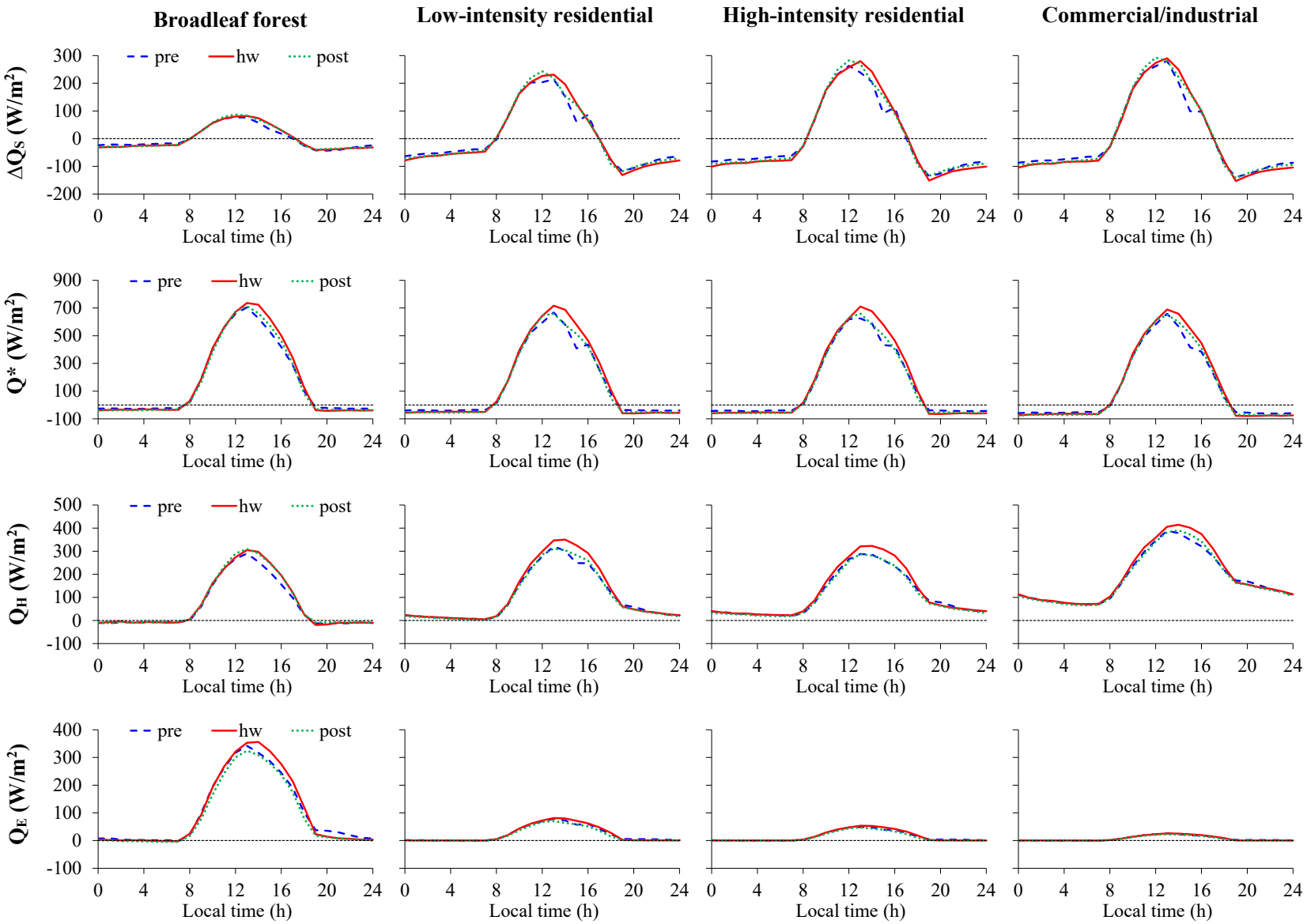
Broadleaf forest
Low-intensity residential
High-intensity residential
Commercial/industrial
pre
hw
post
ΔQS (W/m2)
Q* (W/m2)
QH (W/m2)
QE (W/m2)
Local time (h)

Figure 13. Spatially averaged net heat storage flux (ΔQ_S), net all-wave radiation (Q^*), sensible heat flux (Q_H), and latent heat flux (Q_E) during pre-heat wave ("pre"), heat wave ("hw"), and post-heat wave ("post") for rural (broadleaf forest) and urban categories (low-intensity residential, high-intensity residential, and commercial/industrial areas). Note the different scales for ΔQ_S, Q^*, Q_H, and Q_E.

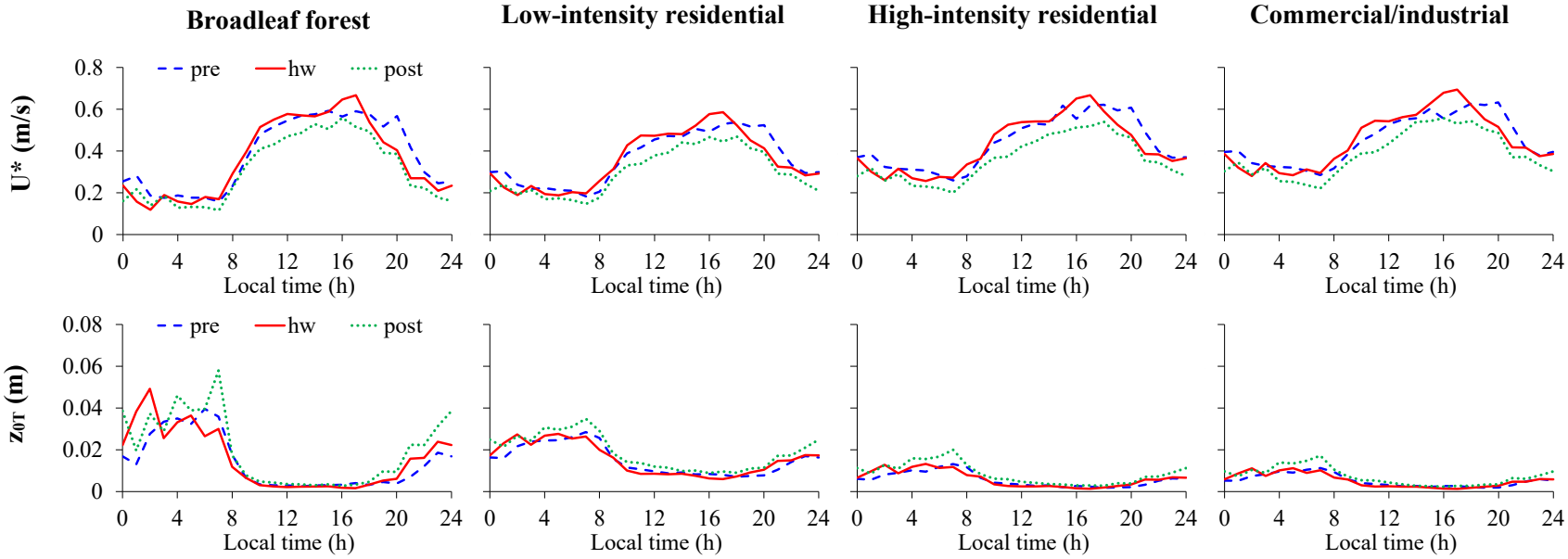

Figure 14. Spatially averaged friction velocity (U^*) and thermal roughness length (z_{0T}) during pre-heat wave ("pre"), heat wave ("hw"), and post-heat wave ("post") for rural (broadleaf forest) and urban categories (low-intensity residential, high-intensity residential, and commercial/industrial areas).

3.5.4 Roughness Lengths and Surface Resistance

As the UHI intensity is sensitive to the roughness lengths (both momentum and thermal) and the surface resistance, it is worthwhile exploring whether the heat wave has affected any of these parameters. The 2-m air temperature, T_2, is a diagnostic variable calculated as:

$$(T_S - T_2) = \frac{Q_H}{\rho C_{h2} U_2} \quad (1)$$

where T_S is the surface temperature; Q_H is the sensible heat flux, ρ is the air density, and C_{h2} and U_2 are the transfer coefficient and wind speed at 2 m (Li and Bou-Zeid, 2014). From the Monin–Obukhov Similarity Theory (Monin and Obukhov, 1954):

$$C_{h2} = \frac{\kappa^2}{\left[ln\left(\frac{2}{z_0}\right) - \psi_m\left(\frac{2}{L}\right)\right]\left[ln\left(\frac{2}{z_{0T}}\right) - \psi_h\left(\frac{2}{L}\right)\right]} \quad (2)$$

where κ is the von Kármán constant, z_0 is the momentum roughness length; z_{0T} is the thermal roughness length; L is the Obukhov length scale; ψ_m is a correction function for momentum; and ψ_h is a correction function for heat. In WRF, z_0 depends only on the land use/land cover type and does not change throughout the simulation but z_{0T} can change with time. The Mellor-Yamada-Janjić PBL scheme parameterizes z_{0T} as:

$$z_{0T} = z_0 e^{-0.1\kappa\sqrt{Re}} \quad (3)$$

where $Re = z_0 U^*/\nu$ is the roughness Reynolds number based on the friction velocity U^* and ν is the kinematic viscosity of air. Given that z_0 and ν are constants, z_{0T} depends only on U^*. Figure 14 plots the spatially averaged U^* and z_{0T} of the rural and urban categories. The diurnal profiles show that the heat wave has no significant effects on U^* and therefore, z_{0T} is not altered during the heat wave. Consequently, C_{h2} is also not affected by the heat wave in both rural and urban areas.

The surface resistance, R_c, is the resistance of water vapour flowing through evapotranspiration. Due to a high fraction of impervious surfaces, urban areas have larger R_c and lower rate of evapotranspiration than rural areas, which in turn induces the UHI effects (Atkinson, 2003). Following Chen & Dudhia (2001) and Jacquemin & Noilhan (1990), R_c is calculated as:

$$R_C = \frac{R_{cmin}}{(LAI)F_1F_2F_3F_4} \quad (4)$$

where R_{cmin} is the minimum resistance; LAI is the leaf area index; F_1, F_2, F_3 and F_4 are the fractional conductances (between 0 and 1) representing the effects of solar radiation, vapor

pressure deficit, air temperature, and soil moisture. The parameterizations of F_1-F_4 are provided in both references (Chen and Dudhia, 2001; Jacquemin and Noilhan, 1990). Overall, the combined effects of F_1-F_4 are not sensitive to the heat wave, as the daytime-averaged R_c of the rural area are 36.7, 34.6, and 36.3 s m^{-1} during the pre-, heat wave, and post-heat wave periods, respectively, close to the typical R_c of 50 s m^{-1} for rural areas (Atkinson, 2003). The nighttime-averaged R_c is about 650 s m^{-1} during all three periods. The nighttime R_c is much larger than the daytime R_c because F_1 becomes very small (~0.006) due to the absence of solar radiance during nighttime. Urban areas have much larger R_c than rural areas due to the large fraction of impervious surface (where R_c is infinitely large). During both the heat wave and non-heat wave periods, low-intensity residential areas, high-intensity residential areas, and commercial or industrial areas have daytime R_c of about 700, 1100, and 2200 s m^{-1}, respectively. During nighttime, R_c exceeds 10,000 s m^{-1} for all three urban categories. Overall, no significant change of R_c is observed during the heat wave in our study.

4. Limitations and Future Work

This study adopted the anthropogenic heat data in Quah and Roth (2012), which estimated the anthropogenic heat from traffic, buildings, and human for 2008 and 2009. During a heat wave, the cooling demand for buildings is expected to surge (Li, 2018), thereby increasing anthropogenic heat from buildings. Using anthropogenic heat data derived from non-heat wave years can cause under-prediction of UHI intensity. Unfortunately, there is no available anthropogenic heat data for Singapore during extreme events. Quantifying anthropogenic heat during a heat wave in tropical cities like Singapore and its effects on UHI intensity can be carried out to obtain more accurate inputs for further studies.

We adopted the single-layer urban canopy model, which does not resolve the height variability of buildings within the same urban land use type and allows only a fixed profile of anthropogenic heat. On the other hand, the more complex multi-layer urban canopy model can explicitly resolve anthropogenic heat released from buildings through building effect parameterization and building energy modeling (Jandaghian and Berardi, 2020b; Mughal et al., 2019). The single-layer urban canopy model also tends to underestimate latent heat flux (Liu et al., 2017). Improved urban canopy models, such as the Princeton Urban Canopy Model (Li and Bou-Zeid, 2014), can also improve the performance of WRF in predicting UHI. Given the highly non-linear interactions of multiple parameters in urban climate modeling, more complex models do not guarantee improvements in accuracy (Grimmond et al., 2011; Salamanca et al.,

2011). However, since there are relatively few studies focusing on the tropics, it is worthwhile to extend the study of heat wave-UHI interaction using more complex models, especially on the modeling of anthropogenic heat and latent heat during heat waves in tropical cities, which can be very different than those of cities in the temperate climate zone.

Our study is limited towards a tropical coastal city and should not be generalized to other tropical cities. Furthermore, this is a case study based on a single heat wave event so the conclusions may be different if we examine more events as an ensemble. For example, Li and Bou-Zeid (2013) showed synergistic effects between UHI and a heat wave event in Baltimore, but the ensemble study in Scott et al. (2018) found no such effects in Baltimore. Nonetheless, this limitation could be a strength: it can motivate more future studies of heat waves in the tropics. Argüeso et al. (2016) have warned that our current knowledge is biased towards the heat waves in North America and Europe. The findings in our case study hypothesize that heat wave-UHI synergy in a tropical city is weaker than that in the mid-latitude cities.

5. Conclusion

The April 2016 heat wave in Singapore was studied using ground observations and the Weather Research and Forecasting (WRF) model. Two weather stations, one in an urban area and one in a rural area (Figure 1), were used to calculate the UHI intensity during the pre-heat wave (April 3-5), heat wave (April 17-19), and post-heat wave (April 24-26) periods. The key findings are:

- The temperatures measured at both stations showed that during the heat wave, daytime temperatures could be 3 °C higher than those during the pre- and post-heat wave periods.
- Despite the temperature spike, the heat wave did not amplify the UHI intensity, where the UHI peaks reach about 2.5 °C during both heat wave and non-heat wave periods.
- WRF simulation results agree well with measurements in predicting both the diurnal profile and the peak UHI.
- WRF simulation results show no heat wave-UHI synergy, consistent with the measurements.
- The spatially averaged UHI intensity of all urban areas in Singapore also shows no heat wave-UHI synergy.

We explored four major factors that contribute to the UHI effect: wind speeds, soil moisture availability, heat storage flux, and the roughness lengths and surface resistance. No

wind speed reduction was observed during the heat wave. The urban-rural soil moisture deficit was not significantly altered during the heat wave. The heat storage flux was not amplified during the heat wave. The roughness lengths and surface resistance were not altered during the heat wave. Despite the higher temperature during the heat wave, all four aforementioned factors remain relatively unchanged during the heat wave. Consequently, no amplification of UHI intensity was observed during the heat wave.

Contrary to some studies in the literature that showed positive synergy between heat waves and UHI, we observe no such synergy for the heat wave in April 2016 in Singapore. The current understanding of heat waves has been biased towards cities in the temperate climate zones. We hope that our study of a tropical city can narrow this gap and motivate future studies of heat waves in the tropics, which are projected to have the largest increase of heat stress in a warming climate.

Acknowledgment

This work is supported by the National Research Foundation Singapore (NRF) under its Campus for Research Excellence and Technological Enterprise (CREATE) program and Intra-CREATE Collaborative Project "Cooling Singapore." The Center for Environmental Sensing and Modeling (CENSAM) is an interdisciplinary research group of the Singapore-MIT Alliance for Research and Technology (SMART). We thank Dr. Wenhui He for helping to process some of the graphics.

References

Ao, X., Wang, L., Zhi, X., Gu, W., Yang, H., Li, D., 2019. Observed Synergies between Urban Heat Islands and Heat Waves and Their Controlling Factors in Shanghai, China. J. Appl. Meteorol. Climatol. 58, 1955–1972.

Argüeso, D., Di Luca, A., Perkins-Kirkpatrick, S.E., Evans, J.P., 2016. Seasonal mean temperature changes control future heat waves. Geophys. Res. Lett. 43, 7653–7660.

Atkinson, B., 2003. Numerical modelling of urban heat-island intensity. Bound.-Layer Meteorol. 109, 285–310.

Basara, J.B., Basara, H.G., Illston, B.G., Crawford, K.C., 2010. The impact of the urban heat island during an intense heat wave in Oklahoma City. Adv. Meteorol. 2010.

Basara, J.B., Hall Jr, P.K., Schroeder, A.J., Illston, B.G., Nemunaitis, K.L., 2008. Diurnal cycle of the Oklahoma City urban heat island. J. Geophys. Res. Atmospheres 113.

Black, E., Blackburn, M., Harrison, G., Hoskins, B., Methven, J., 2004. Factors contributing to the summer 2003 European heatwave. Weather 59, 217–223.

Bohnenstengel, S., Evans, S., Clark, P.A., Belcher, S., 2011. Simulations of the London urban heat island. Q. J. R. Meteorol. Soc. 137, 1625–1640.

Chen, F., Dudhia, J., 2001. Coupling an advanced land surface–hydrology model with the Penn State–NCAR MM5 modeling system. Part I: Model implementation and sensitivity. Mon. Weather Rev. 129, 569–585.

Coumou, D., Rahmstorf, S., 2012. A decade of weather extremes. Nat. Clim. Change 2, 491.

Dousset, B., Gourmelon, F., Laaidi, K., Zeghnoun, A., Giraudet, E., Bretin, P., Mauri, E., Vandentorren, S., 2011. Satellite monitoring of summer heat waves in the Paris metropolitan area. Int. J. Climatol. 31, 313–323.

Fischer, E.M., Oleson, K.W., Lawrence, D.M., 2012. Contrasting urban and rural heat stress responses to climate change. Geophys. Res. Lett. 39.

Fischer, E.M., Schär, C., 2010. Consistent geographical patterns of changes in high-impact European heatwaves. Nat. Geosci. 3, 398.

Fischer, E.M., Seneviratne, S.I., Vidale, P.L., Lüthi, D., Schär, C., 2007. Soil moisture–atmosphere interactions during the 2003 European summer heat wave. J. Clim. 20, 5081–5099.

Founda, D., Santamouris, M., 2017. Synergies between urban heat island and heat waves in Athens (Greece), during an extremely hot summer (2012). Sci. Rep. 7, 10973.

Grimmond, C.S.B., Blackett, M., Best, M.J., Baik, J.-J., Belcher, S., Beringer, J., Bohnenstengel, S., Calmet, I., Chen, F., Coutts, A., others, 2011. Initial results from Phase 2 of the international urban energy balance model comparison. Int. J. Climatol. 31, 244–272.

Guo, Y., Gasparrini, A., Li, S., Sera, F., Vicedo-Cabrera, A.M., Coelho, M. de S.Z.S., Saldiva, P.H.N., Lavigne, E., Tawatsupa, B., Punnasiri, K., others, 2018. Quantifying excess deaths related to heatwaves under climate change scenarios: A multicountry time series modelling study. PLoS Med. 15, e1002629.

He, X., Wang, J., Feng, J., Yan, Z., Miao, S., Zhang, Y., Xia, J., 2020. Observational and modeling study of interactions between urban heat island and heatwave in Beijing. J. Clean. Prod. 247, 119169.

Hirschi, M., Seneviratne, S.I., Alexandrov, V., Boberg, F., Boroneant, C., Christensen, O.B., Formayer, H., Orlowsky, B., Stepanek, P., 2011. Observational evidence for soil-moisture impact on hot extremes in southeastern Europe. Nat. Geosci. 4, 17.

Im, E.-S., Pal, J.S., Eltahir, E.A., 2017. Deadly heat waves projected in the densely populated agricultural regions of South Asia. Sci. Adv. 3, e1603322.

Jacquemin, B., Noilhan, J., 1990. Sensitivity study and validation of a land surface parameterization using the HAPEX-MOBILHY data set. Bound.-Layer Meteorol. 52, 93–134.

Jandaghian, Z., Berardi, U., 2020a. Comparing urban canopy models for microclimate simulations in Weather Research and Forecasting Models. Sustain. Cities Soc. 55, 102025.

Jandaghian, Z., Berardi, U., 2020b. Analysis of the cooling effects of higher albedo surfaces during heat waves coupling the Weather Research and Forecasting model with building energy models. Energy Build. 207, 109627.

Jiang, S., Lee, X., Wang, J., Wang, K., 2019. Amplified urban heat islands during heat wave periods. J. Geophys. Res. Atmospheres 124, 7797–7812.

Kottek, M., Grieser, J., Beck, C., Rudolf, B., Rubel, F., 2006. World map of the Köppen-Geiger climate classification updated. Meteorol. Z. 15, 259–263.

Kotthaus, S., Grimmond, C.S.B., 2014. Energy exchange in a dense urban environment–Part I: Temporal variability of long-term observations in central London. Urban Clim. 10, 261–280.

Kusaka, H., Kimura, F., 2004. Coupling a single-layer urban canopy model with a simple atmospheric model: Impact on urban heat island simulation for an idealized case. J. Meteorol. Soc. Jpn. Ser II 82, 67–80.

Kusaka, H., Kondo, H., Kikegawa, Y., Kimura, F., 2001. A simple single-layer urban canopy model for atmospheric models: Comparison with multi-layer and slab models. Bound.-Layer Meteorol. 101, 329–358.

Li, D., Bou-Zeid, E., 2013. Synergistic interactions between urban heat islands and heat waves: The impact in cities is larger than the sum of its parts. J. Appl. Meteorol. Climatol. 52, 2051–2064.

Li, D., Bou-Zeid, E., 2014. Quality and sensitivity of high-resolution numerical simulation of urban heat islands. Environ. Res. Lett. 9, 055001.

Li, D., Sun, T., Liu, M., Wang, L., Gao, Z., 2016. Changes in wind speed under heat waves enhance urban heat Islands in the Beijing metropolitan area. J. Appl. Meteorol. Climatol. 55, 2369–2375.

Li, D., Sun, T., Liu, M., Yang, L., Wang, L., Gao, Z., 2015. Contrasting responses of urban and rural surface energy budgets to heat waves explain synergies between urban heat islands and heat waves. Environ. Res. Lett. 10, 054009.

Li, X., Zhang, C., Li, W., Ricard, R., Meng, Q., Zhang, W., 2015. Assessing street-level urban greenery using Google Street View and a modified green view index. Urban For. Urban Green. 14, 675–685.

Li, X.-X., 2020. Heat wave trends in Southeast Asia during 1979–2018: The impact of humidity. Sci. Total Environ. 721, 137664.

Li, X.-X., 2018. Linking residential electricity consumption and outdoor climate in a tropical city. Energy 157, 734–743.

Li, X.-X., Koh, T.-Y., Entekhabi, D., Roth, M., Panda, J., Norford, L.K., 2013. A multi-resolution ensemble study of a tropical urban environment and its interactions with the background regional atmosphere. J. Geophys. Res. Atmospheres 118, 9804–9818.

Li, X.-X., Koh, T.-Y., Panda, J., Norford, L.K., 2016. Impact of urbanization patterns on the local climate of a tropical city, Singapore: An ensemble study. J. Geophys. Res. Atmospheres 121, 4386–4403.

Li, X.-X., Norford, L.K., 2016. Evaluation of cool roof and vegetations in mitigating urban heat island in a tropical city, Singapore. Urban Clim. 16, 59–74.

Lin, M., 2016. Lower production at Malaysian farms due to drought pushes up market prices here. Straits Times, https://www.straitstimes.com/singapore/vegetable-prices-rise-on-heatwave (accessed 10.13.18).

Liu, X., Li, X.-X., Harshan, S., Roth, M., Velasco, E., 2017. Evaluation of an urban canopy model in a tropical city: the role of tree evapotranspiration. Environ. Res. Lett. 12, 094008.

Meehl, G.A., Tebaldi, C., 2004. More intense, more frequent, and longer lasting heat waves in the 21st century. Science 305, 994–997.

Meteorological Service Singapore, 2017. Annual climatological report 2016. Centre for Climate Research Singapore.

Meteorological Service Singapore, 2020. Meteorological Service Singapore Homepage, http://www.weather.gov.sg (accessed 6.17.20).

Miller, N.L., Hayhoe, K., Jin, J., Auffhammer, M., 2008. Climate, extreme heat, and electricity demand in California. J. Appl. Meteorol. Climatol. 47, 1834–1844.

Monin, A.S., Obukhov, A.M., 1954. Basic laws of turbulent mixing in the surface layer of the atmosphere. Contrib Geophys Inst Acad Sci USSR 151, e187.

Mora, C., Dousset, B., Caldwell, I.R., Powell, F.E., Geronimo, R.C., Bielecki, C.R., Counsell, C.W., Dietrich, B.S., Johnston, E.T., Louis, L.V., et al., 2017. Global risk of deadly heat. Nat. Clim. Change 7, 501.

Mughal, M.O., Li, X.-X., Yin, T., Martilli, A., Brousse, O., Dissegna, M.A., Norford, L.K., 2019. High-resolution, multi-layer modelling of Singapore's urban climate incorporating local climate zones. J. Geophys. Res. Atmospheres. https://doi.org/10.1029/2018JD029796

National Centers for Environmental Prediction, 2015. NCEP GDAS/FNL 0.25 Degree Global Tropospheric Analyses and Forecast Grids. Research Data Archive at the National Center for Atmospheric Research, Computational and Information Systems Laboratory, Boulder CO.

Ng, L., 2019. A City in a Garden, in: Dense and Green Building Typologies. Springer, pp. 5–6.

Offerle, B., Grimmond, C.S.B., Fortuniak, K., K\lysik, K., Oke, T.R., 2006. Temporal variations in heat fluxes over a central European city centre. Theor. Appl. Climatol. 84, 103–115.

Oke, T.R., 1988. The urban energy balance. Prog. Phys. Geogr. 12, 471–508.

Perkins, S., Alexander, L., Nairn, J., 2012. Increasing frequency, intensity and duration of observed global heatwaves and warm spells. Geophys. Res. Lett. 39.

Quah, A.K., Roth, M., 2012. Diurnal and weekly variation of anthropogenic heat emissions in a tropical city, Singapore. Atmos. Environ. 46, 92–103.

Ramamurthy, P., Bou-Zeid, E., 2017. Heatwaves and urban heat islands: a comparative analysis of multiple cities. J. Geophys. Res. Atmospheres 122, 168–178.

Ramamurthy, P., Li, D., Bou-Zeid, E., 2017. High-resolution simulation of heatwave events in New York City. Theor. Appl. Climatol. 128, 89–102.

Rastogi, D., Lehner, F., Ashfaq, M., 2020. Revisiting recent US heat waves in a warmer and more humid climate. Geophys. Res. Lett. 47, e2019GL086736.

Ratti, C., Seiferling, I., Li, X., Ghaeli, N., So, W., 2016. Exploring the Green Canopy in cities around the world. Treepedia, http://senseable.mit.edu/treepedia (accessed 4.5.20).

Rizwan, A.M., Dennis, Y.C.L., Liu, C., 2008. A review on the generation, determination and mitigation of Urban Heat Island. J. Environ. Sci. 20, 120–128.

Salamanca, F., Martilli, A., Tewari, M., Chen, F., 2011. A study of the urban boundary layer using different urban parameterizations and high-resolution urban canopy parameters with WRF. J. Appl. Meteorol. Climatol. 50, 1107–1128.

Schatz, J., Kucharik, C.J., 2015. Urban climate effects on extreme temperatures in Madison, Wisconsin, USA. Environ. Res. Lett. 10, 094024.

Scott, A.A., Waugh, D.W., Zaitchik, B.F., 2018. Reduced Urban Heat Island intensity under warmer conditions. Environ. Res. Lett. 13, 064003.

Shin, H.H., Dudhia, J., 2016. Evaluation of PBL parameterizations in WRF at subkilometer grid spacings: Turbulence statistics in the dry convective boundary layer. Mon. Weather Rev. 144, 1161–1177.

Skamarock, W.C., Klemp, J.B., Dudhia, J., Gill, D.O., Barker, D.M., Duda, M.G., Huang, X.-Y., Wang, W., Powers, J.G., 2008. A Description of the Advanced Research WRF Version 3.

Steadman, R.G., 1979. The assessment of sultriness. Part I: A temperature-humidity index based on human physiology and clothing science. J. Appl. Meteorol. 18, 861–873.

Stewart, I.D., 2019. Why should urban heat island researchers study history? Urban Clim. 30, 100484.

Stewart, I.D., 2011. A systematic review and scientific critique of methodology in modern urban heat island literature. Int. J. Climatol. 31, 200–217.

Stewart, I.D., Oke, T.R., 2012. Local climate zones for urban temperature studies. Bull. Am. Meteorol. Soc. 93, 1879–1900.

Sun, T., Kotthaus, S., Li, D., Ward, H.C., Gao, Z., Ni, G.-H., Grimmond, C.S.B., 2017. Attribution and mitigation of heat wave-induced urban heat storage change. Environ. Res. Lett. 12, 114007.

Tapiador, F.J., Navarro, A., Moreno, R., Sánchez, J.L., García-Ortega, E., 2020. Regional climate models: 30 years of dynamical downscaling. Atmospheric Res. 235, 104785.

Timbal, B., Turkington, T., Hassim, M.E., 2018. Temperatures Rising. ENVISION 15, 54–57.

Unger, J., Skarbit, N., Kovács, A., Gál, T., 2020. Comparison of regional and urban outdoor thermal stress conditions in heatwave and normal summer periods: A case study. Urban Clim. 32, 100619.

Valmassoi, A., Dudhia, J., Di Sabatino, S., Pilla, F., 2020. Irrigation impact on precipitation during a heatwave event using WRF-ARW: The summer 2015 Po Valley case. Atmospheric Res. 104951.

Wang, L., Li, D., Gao, Z., Sun, T., Guo, X., Bou-Zeid, E., 2014. Turbulent transport of momentum and scalars above an urban canopy. Bound.-Layer Meteorol. 150, 485–511.

Ward, H., Evans, J.G., Grimmond, C.S.B., 2013. Multi-season eddy covariance observations of energy, water and carbon fluxes over a suburban area in Swindon, UK. Atmospheric Chem. Phys. 13, 4645–4666.

Whitman, S., Good, G., Donoghue, E.R., Benbow, N., Shou, W., Mou, S., 1997. Mortality in Chicago attributed to the July 1995 heat wave. Am. J. Public Health 87, 1515–1518.

Wyngaard, J.C., 2004. Toward numerical modeling in the “Terra Incognita.” J. Atmospheric Sci. 61, 1816–1826.

Zhao, L., Oppenheimer, M., Zhu, Q., Baldwin, J.W., Ebi, K.L., Bou-Zeid, E., Guan, K., Liu, X., 2018. Interactions between urban heat islands and heat waves. Environ. Res. Lett. 13, 034003.